Selective catalytic reduction of nitric oxide by hydrogen over Zn-ZSM-5 and Pd and Pd/Ru based catalysts

Lifeng Wang [a], Hao Chen [a], Min-Hao Yuan [a], Sandrine Rivillon [b,*], Eric H. Klingenberg [b], Jimmy Xianming Li [b], Ralph T. Yang [a,*]

[a] Department of Chemical Engineering, University of Michigan, Ann Arbor, MI 48109, USA
[b] Air Products and Chemicals, Inc., 7201 Hamilton Blvd., Allentown, PA 18195, USA

ARTICLE INFO

ABSTRACT

The catalytic reduction of NO_x with hydrogen (H_2-SCR) in excess oxygen over a non-noble metal catalyst, Zn-ZSM-5, was studied for the first time. The results showed that Zn-ZSM-5 had considerable activity for H_2-SCR, with a single NO_x conversion peak at 250 °C, and high N_2 product selectivity. Two noble metal based catalysts, Pd/Zn-ZSM-5 and Pd/Ru/W/(ZrO_2–SiO_2)SO_4, were also synthesized and their H_2-SCR activities were evaluated and compared with Zn-ZSM-5 under identical laboratory experimental conditions. The effects of CO concentration, water vapor and SO_2 added to the feed gas (NO, H_2, balance He) on H_2-SCR over these three catalysts were also studied and compared. hydrogen temperature programmed desorption (H_2-TPD) experiments were performed on Zn-ZSM-5: the results showed strong chemisorption of hydrogen, while both the amount and the binding strength of the chemisorbed hydrogen increased with the hydrogen dosing temperature. The role of Zn cations in the chemisorption is also discussed.

1. Introduction

Nitrogen oxides (NO_x) are major atmospheric pollutants, which cause photochemical smog, acid rain, ozone depletion and greenhouse effects. Selective catalytic reduction (SCR) technology where NH_3 as a reducing agent reacts with NO_x over a catalyst is the most widely used technology for reducing nitrogen oxide emissions from power plants [1–24]. It is an effective and reliable technology which currently used in stationary and mobile applications; however, this approach comes with issues such as NH_3 slip and "white powder" formation. White powder of ammonium compounds (i.e., bisulfate, sulfate, nitrate...) formed in NH_3-SCR causes equipment fouling and corrosion problems.

One possible alternative approach for SCR is the use of hydrogen as a reductant (H_2-SCR). Because of the high efficiency in NH_3-SCR, studies on alternative reductants such as hydrogen are relatively recent and only few results are reported involving the reaction of hydrogen with nitrous oxide over various noble metal catalyst

supports exhibiting high catalytic activities for H_2-SCR in excess oxygen [25–45]. The use of noble metals significantly increases the cost of these catalysts and prevents H_2-SCR technology to compete with NH_3-SCR. From a practical point of view thus, development of a non-noble metal catalyst for NO_x reduction would be desirable.

It is known that noble metals dissociate hydrogen and an H-assisted NO decomposition mechanism was proposed to explain $NO/H_2/O_2$ reaction over $Pt/La_{0.5}Ce_{0.5}MnO_3$ catalyst studied by Costa et al. [29]. Dissociated hydrogen facilitates the reduction of NO. For development of a non-noble metal catalyst for H_2-SCR, a non-noble metal which can dissociate hydrogen seems a promising path forward.

It has been reported by Iglesia et al. that Zn facilitated dissociative adsorption of H_2 on ZSM-5 in their isotopic studies of H_2/D_2 equilibration during propane aromatization and alkane dehydrogenation mechanism [46,47]. DRIFTS results by Kazansky et al. also showed dissociative adsorption of H_2 on Zn-ZSM-5 [48–50]. Considering the strong interactions between H_2 and Zn-ZSM-5, Zn-ZSM-5 could be thus a potential catalyst for the H_2-SCR reaction. Herein, we synthesized Zn-ZSM-5 catalyst and studied its performance for NO reduction with H_2 over a range of temperature from 100 to 350 °C and H_2/NO ratio. In addition, H_2-SCR activities over two noble metal catalysts, Pd/Zn-ZSM-5 and Pd/Ru/W/(ZrO_2–SiO_2)SO_4 (synthesized by Siemens Corporation) [51] were also evaluated and compared with Zn-ZSM-5 under

* Corresponding authors at: College of Engineering, University of Michigan, 2300 Hayward, Ann Arbor, MI 48109-2136, USA. Tel.: +1 7349360771; fax: +1 7347647453.
E-mail addresses: rivills@airproducts.com (S. Rivillon), yang@umich.edu (R.T. Yang).

identical experimental conditions. The effects of CO, water vapor and sulfur dioxide on the catalytic activities over these catalysts were also investigated to determine the stability of the catalyst for stationary and mobile applications. Finally H_2-TPD experiments were performed on Zn-ZSM-5 to understand the chemisorptions process on Zn-ZSM-5 when hydrogen molecules are present in the feed gas.

2. Experimental

2.1. Catalysts preparation

2.1.1. Zn-ZSM-5 catalyst

Ammonium form of ZSM-5 zeolite with framework Si/Al ratio of 25 was calcined in air at 500 °C for 5 h to obtain H form of ZSM-5. 0.5 g of H form of ZSM-5 zeolite was then ion exchanged with 50 mL of $Zn(NO_3)_2$ (0.01 M) solution at 80 °C overnight. Zn-ZSM-5 zeolite was collected by centrifugation, washed with deionized water, and dried in oven at 110 °C and treated *in vacuum* at 350 °C for 24 h. To optimize the concentration of zinc in ZSM-5, Zn-ZSM-5, Zn-ZSM-5-2, Zn-ZSM-5-3 and Zn-ZSM-5-4 samples were also prepared by the ion-exchange procedure, respectively, once, twice, three times and fourth times. Zn-ZSM-5-5 was also prepared by doping Zn-ZSM-5-4 with 2 wt% ZnO via incipient wetness impregnation of $Zn(NO_3)_2$.

2.1.2. 1 wt% Pd/Zn-ZSM-5 catalyst

The 1 wt% Pd/Zn-ZSM-5 was prepared via incipient wetness impregnation (IWI) of Zn-ZSM-5 in an aqueous solution of $Pd(NH_3)_4Cl_2$. The solid sample was then dried at 120 °C for 12 h and calcined in air at 500 °C for 6 h.

We also synthesized Pd/Zn-ZSM-5-plasma sample by using the glow discharge plasma reduction route. After IWI of Zn-ZSM-5 with $Pd(NH_3)_4Cl_2$, the composite was loaded on a quartz boat that was placed in the glow discharge cell. When the pressure was adjusted to the range of 1000–2000 mTorr, the glow discharge plasma was generated by applying 3.1 kV to the electrodes using a dc high-voltage generator with Ar as the plasma-forming gas.

2.1.3. Pd/Ru/W/(ZrO₂–SiO₂)SO₄ catalyst

The synthesis of $Pd/Ru/W/(ZrO_2–SiO_2)SO_4$ was carried out following the similar procedure described in Example 3 of US Patent 7,976,805, except that no monolith core (honeycomb support) was used in our synthesis [51]. 0.8% Pd and 0.11% Ru were added via incipient wetness impregnation method during the synthesis. The IWI method allowed good control of the loading amounts of metal dopants in the final product, in which the loading amounts were the same as the starting ratios in the synthesis slurry (as all solvents were evaporated). All chemical reagents were purchased from Aldrich.

2.2. Characterization and catalytic tests

The powder X-ray diffraction (XRD) measurements were carried out with a Rigaku Rotaflex D/Max-C system with Cu $K\alpha$ (λ = 0.1543 nm) radiation. Micromeritics ASAP 2020 micropore size analyzer was used to measure the N_2 adsorption isotherms of the samples at liquid N_2 temperature (−196 °C). The specific surface area was determined from the linear portion of the BET plot. Prior to the surface area and pore size distribution measurements, the samples were degassed in vacuum at 350 °C for 24 h. Zn contents in Zn-ZSM-5 and Zn-Y were measured with EDX affiliated Phillips XL30 FEG SEM. Zn-Y was synthesized following the same synthesis procedure of Zn-ZSM-5 for TPD study.

The catalytic activity measurement was carried out in a fixed-bed quartz reactor. The reactant gas composition was: 50–200 ppm NO, 0–3000 ppm H_2, 0–2000 ppm CO, 1.5% O_2, and balance He.

Water vapor and SO_2 were also added to the feed gas to study the effect of water vapor and SO_2 on the NO_x reduction over these catalysts. A 200–250 mg of sample was used in each run. The total flow rate was 100 or 200 mL/min (under ambient conditions). The NO and NO_2 concentrations were continually monitored using a chemiluminescent NO/NO_x analyzer (Thermo Environmental Instruments, Inc.). The products were also analyzed using Shimadzu gas chromatographs with 13× molecular sieve column for H_2, CO and N_2 separation and Porapak Q column for N_2O. The catalytic activity was based on the calculated NO_x ($NO + NO_2$) conversion. At each reaction temperature, the NO_x conversion and product analysis were measured after 1–2 h (for reaching steady state) depending on the reaction.

2.3. H₂-TPD measurements

Hydrogen Temperature Programmed Desorption (H_2-TPD) spectra were measured with an AeroVac 1200 Magnetic Sector mass spectrometer (VTI, Inc.), operated at an accelerating voltage of 70 eV. The detailed description of the TPD apparatus was given in previous works [52–54]. As a typical run, 120 mg of sample was placed in a stainless steel holder and degassed in vacuum at 350 °C overnight until the pressure in the system was lower than 5×10^{-8} Torr. Then the sample was cooled down to 0 or 25 or 50 °C, dosed with pre-dried ultrahigh purity hydrogen at the pressure of 750 Torr and allowed to reach equilibrium after a period of time at corresponding temperature. After reaching equilibrium, the sample holder was immersed and quenched in liquid nitrogen. The system was then slowly degassed until the pressure dropped down lower than 10^{-6} Torr to remove excess gas and hydrogen level were at the background. After that, the sample was heated at a constant rate of 10 or 15 or 20 °C/min from −196 to 350 °C, while the effluent gas was monitored with a mass spectrometer.

3. Results and discussion

3.1. Characterization of Zn-ZSM-5 and H2-TPD studies

Zn-ZSM-5 was obtained by ion exchanging H-ZSM-5 zeolites with $Zn(NO_3)_2$ between one and four times. The XRD pattern of Zn-ZSM-5 ion-exchanged once is shown in Fig. S1. The obtained Zn-ZSM-5 exhibited the characteristic of peaks associated with MFI structure, indicating the zeolite structure was retained after the ion exchange process (See the Supporting information). N_2 adsorption isotherm of Zn-ZSM-5 was a typical type I isotherm and the results showed the BET surface area of Zn-ZSM-5 being high: 420 m²/g (Fig. S2). EDX results determined that 1.17% Zn was exchanged in Zn-ZSM-5 (not shown). We also tested the hydrothermal stability of Zn-ZSM-5 by treating the sample in boiling water for 24 h. The nitrogen adsorption results showed that the BET surface area of one time treated Zn-ZSM-5 is 403 m²/g which is closed to 420 m²/g of the untreated one. These results confirm Zn-ZSM-5 is hydrothermally stable.

H_2-TPD experiments were conducted to investigate the interactions between hydrogen and Zn-ZSM-5 (Table 1). Fig. 1a shows the H_2-TPD curves with a heating rate of 10 °C/min for Zn-ZSM-5, which was dosed with hydrogen at temperatures of 0, 25 and 50 °C. Two TPD peaks were observed (Fig. 1a). The first one around −150 °C was assigned to physisorption of H_2 molecules on the surface of Zn-ZSM-5. The second peak in the range of 100–200 °C was attributed to strongly chemisorbed hydrogen on Zn-ZSM-5. Unlike the peak associated to H_2 physisorption which remained almost unchanged with dosing temperature, the temperature of the second peak and its intensity and area increased with the dosing temperature suggesting that more hydrogen was chemisorbed on Zn-ZSM-5 as the

Table 1
TPD experiment conditions, peak intensity, maximum peak temperature and peak area of Zn-ZSM-5, Zn–Y, H-ZSM-5 and H–Y samples exposed to hydrogen.

Sample	Heating rate (°C/min)	Dosing temperature (°C)	Peak temperature (°C)	Peak maximum intensity (chemisorption)	Peak area (chemisorption)
Zn-ZSM-5	10	0	107	2.2E − 09	2.2E − 07
Zn-ZSM-5	10	25	125	2.7E − 09	2.5E − 07
Zn-ZSM-5	10	50	166	3.5E − 09	3.2E − 07
Zn-ZSM-5	15	0	125	3.1E − 09	2.9E − 07
Zn-ZSM-5	15	25	147	3.6E − 09	3.2E − 07
Zn-ZSM-5	15	50	175	4.6E − 09	3.8E − 07
Zn-ZSM-5	20	0	152	3.9E − 09	4.2E − 07
Zn-ZSM-5	20	25	174	4.4E − 09	4.6E − 07
Zn-ZSM-5	20	50	195	7.4E − 09	7.3E − 07
H-ZSM-5	10	25	N/A	N/A	N/A
H-ZSM-5	20	25	N/A	N/A	N/A
Zn–Y	20	25	143	1.90E − 09	1.1E − 07
H–Y	20	25	N/A	N/A	N/A

dosing temperature increased. A similar favorable effect of temperature was also reported in DRIFT study by Kazansky [48], who observed the increased dissociative adsorption of hydrogen with temperature increasing from 293 to 473 K. As mentioned, higher dosing temperature caused a shift of the TPD peak to higher temperature, indicating that the activation energy for desorption increased with dosing temperature. Similar trend was also observed when the heating rate of TPD was changed to 15 and 20 °C/min and the results are shown in Fig. 1b and c.

It was also found that higher heating rates led to higher peak intensity and the shifts of TPD peaks to higher temperature
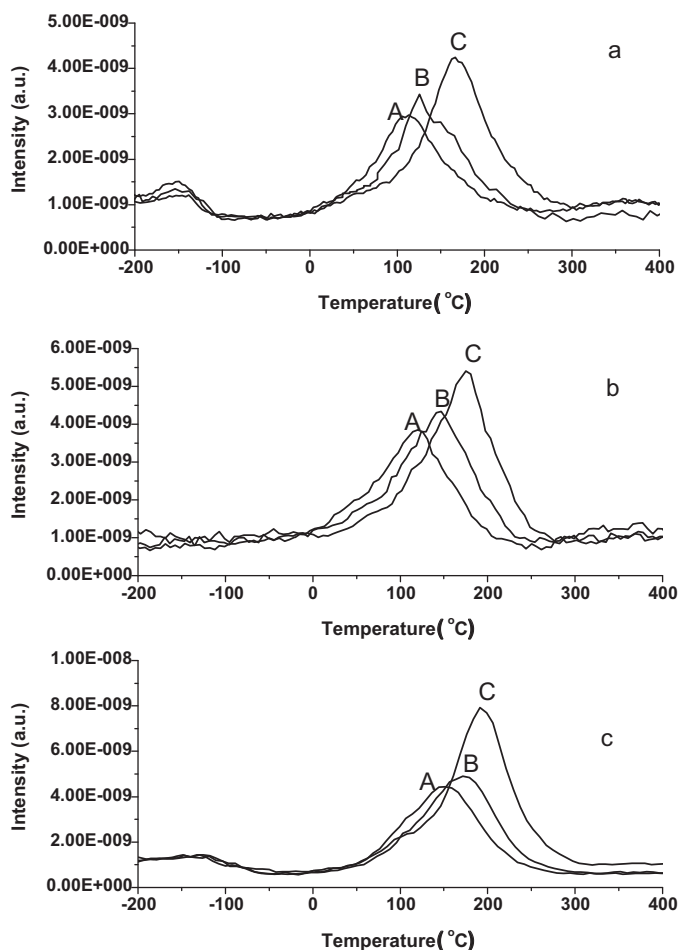

Fig. 1. H$_2$-TPD curves (heating rate (a) 10 °C/min; (b) 15 °C/min; (c) 20 °C/min) for Zn-ZSM-5 dosed with H$_2$ at (A) 0, (B) 25, and (C) 50 °C.

positions, which are consistent with previous TPD studies [55–57]. For example, when Zn-ZSM-5 was dosed with hydrogen at 50 °C followed by TPD at a heating rate of 10 °C/min, the peak maximum temperature (T_m) for the chemisorbed hydrogen was 166 °C; this value is increased to 175 °C at a heating rate of 15 °C/min and 195 °C at a heating rate of 20 °C/min, respectively. Meanwhile, the peak intensity increased from 3.5×10^{-9} at heating rate of 10 °C/min to 4.6×10^{-9} at 15 °C/min, and 7.4×10^{-9} at 20 °C/min: with higher heating rate, more energy was brought to the system per time unit breaking the strong interaction between chemisorbed hydrogen and Zn-ZSM-5, releasing thus more hydrogen per time unit, leading to higher desorption rate (and higher peak intensity).

It is noted that small physically adsorbed hydrogen peaks are sometimes present in the TPD curves. Before TPD analysis, the sample holder was immersed and quenched in liquid nitrogen. The system was then slowly degassed until the pressure dropped to lower than 10^{-6} Torr to remove excess gas and hydrogen level were at the background. This procedure allowed us to remove all the hydrogen gas in the sample holder and most of the physically adsorbed hydrogen. However, due to the small variation of degassing conditions (e.g., degassing time or pressure reader) in the TPD system, sometimes there maybe a small amount of physically adsorbed hydrogen left, but it is likely that most of physically adsorbed hydrogen was removed with pressure lower than 10^{-6} Torr. It is noted that the analysis of the chemically absorbed hydrogen is not affected since their bonding are much stronger and the desorption peak occurred at much higher temperature.

Because of the asymmetry of TPD peaks, the desorption rate is assumed to be first order and the pre-exponential factor and activation energy for desorption are assumed to be independent of surface coverage and heating rates, then the modified Redhead equation can be used to estimate the activation energy for desorption by monitoring T_m change with heating rates [55,58]. The activation energy for desorption was determined by evaluating the slope of a plot of $\ln\left(T_m^2/\beta\right)$ against $1/T_m$ (β is heating rate). The plots are shown in Fig. 2. The activation energies for hydrogen desorption from Zn-ZSM-5 were calculated to be 14.1 kJ/mol with dosing temperature at 0 °C, 15.7 kJ/mol at 25 °C and 30.0 kJ/mol at 50 °C. These results confirmed that higher dosing temperature led to higher activation energy for desorption, i.e., stronger bonds between the chemisorbed hydrogen and the catalyst support.

In order to study the role of Zn in the interaction mechanism between H$_2$ and Zn-ZSM-5, TPD experiments on H-ZSM-5 without zinc cations were also carried out at 25 °C with the heating rate of 20 °C/min. The corresponding TPD curves are shown in Fig. 3A. The only peak of the TPD curve shown in H-ZSM-5 was assigned to the weak physisorption of hydrogen on H-ZSM-5. No peak at higher temperature (chemisorption peak) was observed, which was very
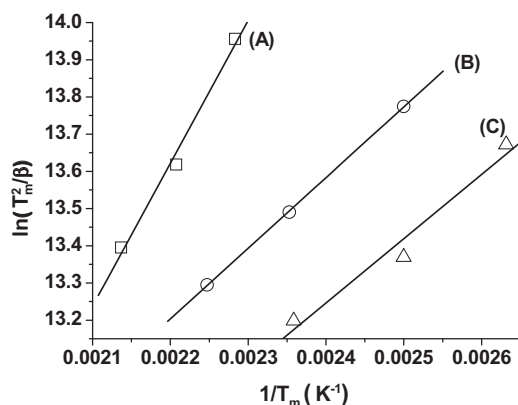
Fig. 2. Redhead plots of $\ln\left(T_m^2/\beta\right)$ against $1/T_m$ for TPD on Zn-ZSM-5 at different hydrogen dosing temperatures: (A) 50, (B) 25, and (C) 0 °C.

different from the results for Zn-ZSM-5. This demonstrated that zinc in ZSM-5 played an important role in the chemisorption of hydrogen on Zn-ZSM-5.

To further verify the role of Zn cations in hydrogen adsorption on Zn-ZSM-5 and also to investigate whether the framework of zeolite affected its interactions with H_2, H_2-TPD experiments were also performed on Zn–Y and H–Y zeolites. The TPD curves of Zn–Y and H–Y dosed with hydrogen at 25 °C are shown in Fig. 3B. As shown in Fig. 3B, no chemisorption peak of hydrogen was observed on H–Y while there was a chemisorption peak on Zn–Y. These results further confirmed that Zn played a determining role in hydrogen chemisorption on zeolites.

TPD curves of Zn-ZSM-5 and Zn–Y were also compared in Fig. 3C. As shown in Fig. 3C and Table 1, the TPD peak area of Zn-ZSM-5 is ~4 times that of Zn–Y. Considering the use of the same amount (120 mg) of Zn-ZSM-5 and Zn–Y samples and the same dosing temperature and heating rate for TPD tests, it is concluded that more hydrogen was chemisorbed on Zn-ZSM-5 than Zn–Y. Note that the peak maximum temperature of TPD on Zn–Y was lower than that on Zn-ZSM-5. This means the interactions between hydrogen and Zn–Y were weaker than the ones between hydrogen and Zn-ZSM-5, which led to more chemisorbed hydrogen on Zn-ZSM-5 than Zn–Y, although Zn content in Zn–Y was higher than that in Zn-ZSM-5. These results demonstrated that the framework of zeolite also affected hydrogen chemisorption on zeolite. TPD results were also in agreement with previous simulation work: periodical density functional theory (DFT) by Barbosa et al. showed that the adsorption and dissociation of hydrogen molecules varied on different Zn exchanged zeolites [59].

3.2. NOx reduction on Zn-ZSM-5 catalyst

The performance of Zn-ZSM-5 catalyst for NO_x reduction with H_2 in the presence of excess oxygen (e.g., 1.5% O_2) was tested. As shown in Fig. 4, Zn-ZSM-5 is an active catalyst for H_2-SCR. At low temperatures, NO_x conversion increased with temperature and reached 39.5% at 250 °C; subsequently NO conversion slightly decreased with temperature being increased to 350 °C. N_2 was the main product for NO_x reduction over Zn-ZSM-5: N_2 selectivity ranging from 70 to 90% was obtained on Zn-ZSM-5 throughout the studied temperature range (Fig. 4). In previous results regarding H_2-SCR using noble metal catalysts (mainly Pt and Pd), the first activity peak occurs at 100–150 °C, which is related directly with H_2 dissociation over noble metal [32]. For Zn-ZSM-5, the activity continues to rise through this temperature range. The increased conversion with temperature was likely due to the increased chemisorption/dissociation activities of Zn-ZSM-5 with temperature, as
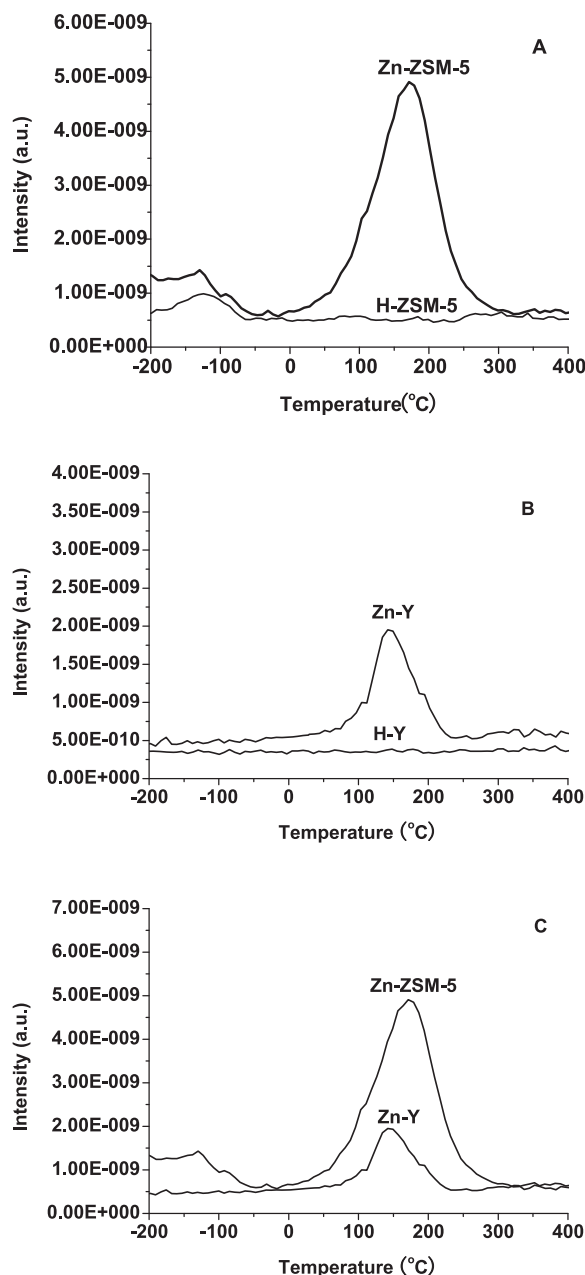

Fig. 3. H_2-TPD curves for (A) H-ZSM-5 and Zn-ZSM-5, (B) Zn–Y and H–Y, and (C) Zn-ZSM-5 and Zn–Y dosed with hydrogen at 25 °C at the heating rate of 20 °C/min (TPD curve of H–Y was offset by 1.5E − 10 for clarity).

shown by the H_2-TPD results; thus, more chemisorbed/dissociated hydrogen was involved in NO reduction. Hydrogen conversion as a function of temperature over Zn-ZSM-5 also supported the observation. As shown in Fig. 4, H_2 conversion over Zn-ZSM-5 reached 100% conversion at the temperature (i.e., 250 °C) where the maximum NO conversion was observed (Fig. 6). At temperature higher than 250 °C, the consumption of H_2 by O_2 became dominant, which caused NO_x conversion to start decreasing (hydrogen conversion indicates the combustion of hydrogen with oxygen). Fig. 5 further showed that when oxygen was absent in the feed gas, NO_x conversion increased from 39.5% to 56.8% at 250 °C and a slight increase in NO_x conversion was observed at temperatures higher than 250 °C confirming the combustion of hydrogen for temperature higher than 250 °C. The removal of oxygen also increased N_2 selectivity (Fig. S3). In the absence of oxygen, more hydrogen is available for the reduction of NO. Additionally when higher
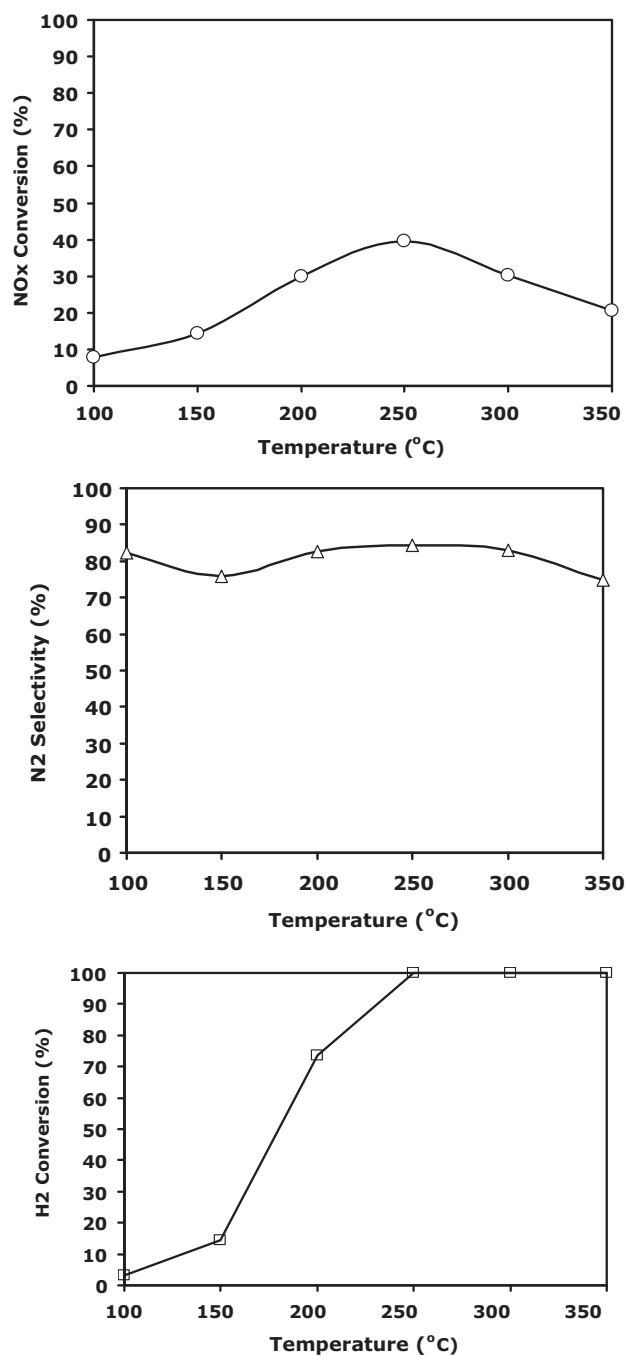
Fig. 5. NO_x conversion over Zn-ZSM-5 as a function of temperature with 1.5 wt% O_2 (○) or without O_2 (△). Reaction condition: 50 ppm NO, 2000 ppm H_2, balance helium, 0.2 g catalyst, flow rate 200 mL/min.

The NO concentration feed was increased from 50 to 200 ppm to test the performance of Zn-ZSM-5 catalyst for NO_x reduction at high NO concentration. As shown in Fig. 7, when NO concentration was increased for a H_2/NO ratio of 15/1, NO_x conversion over Zn-ZSM-5 increased in the whole temperature range, with a maximum for NO_x conversion of 63.3% still achieved at 250 °C, N_2 selectivity was around 70% at temperatures lower than 250 °C and

Fig. 4. NO_x conversion, N_2 selectivity, and hydrogen conversion over Zn-ZSM-5 as a function of temperature. Reaction condition: 50 ppm NO, 2000 ppm H_2, 1.5% O_2, balance helium, 0.2 g catalyst, flow rate 200 mL/min.

concentration of hydrogen (4000 ppm) was added to the feed, higher NO conversion was obtained in the whole temperature range with the highest conversion occurring at 250 °C (Fig. S4).

The effect of space velocity (flow rate) on NO_x reduction is displayed in Fig. 6. It can be seen that space velocity influenced NO_x conversion. As space velocity was decreased from 6×10^4 to 3×10^4 h^{-1} (the total flow rate reduced from 200 to 100 mL/min), NO_x conversion over Zn-ZSM-5 increased in the whole temperature range. At 250 °C, the highest NO_x conversion increased from 39.5% to 55%. Unlike the effect of space velocity on NO_x conversion, no obvious influence of space velocity on N_2 selectivity over Zn-ZSM-5 was observed (Fig. 6).
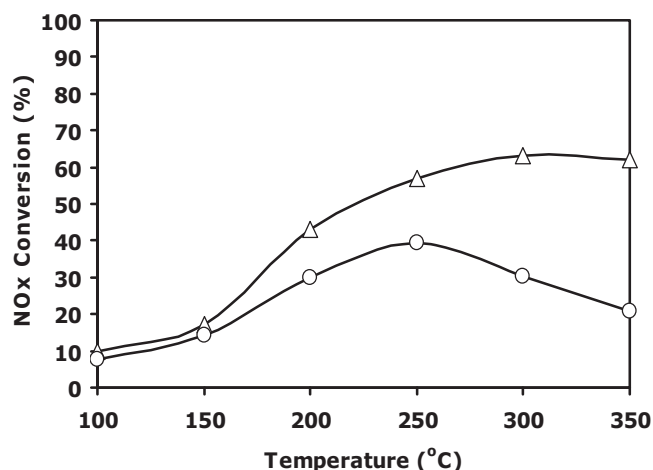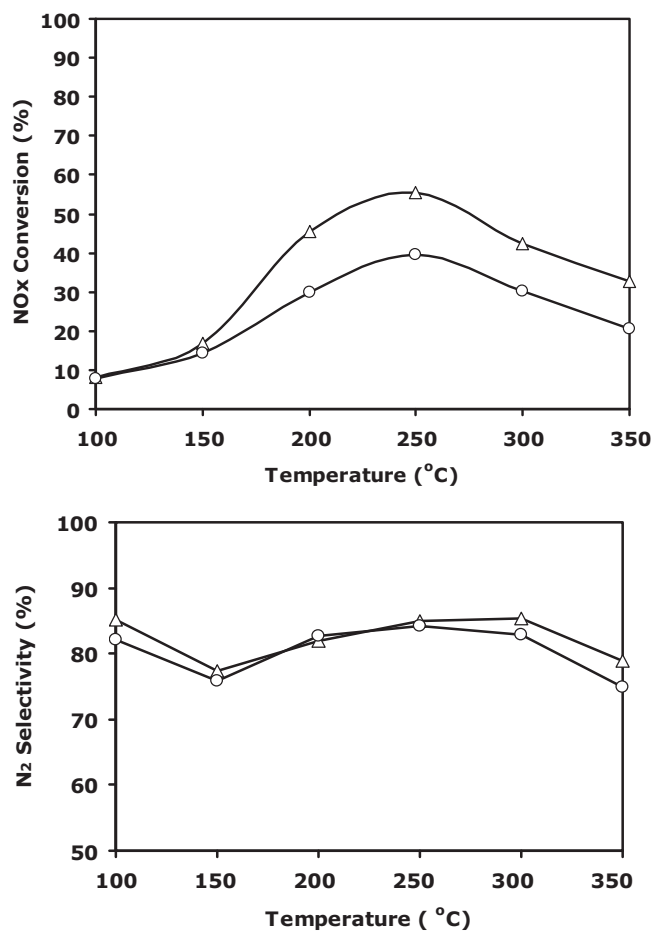

Fig. 6. NO_x conversion and N_2 selectivity over Zn-ZSM-5 as a function of temperature. Reaction condition: 50 ppm NO, 2000 ppm H_2, 1.5% O_2, balance helium, 0.2 g catalyst, flow rates: 100 mL/min (△) and 200 mL/min (○).
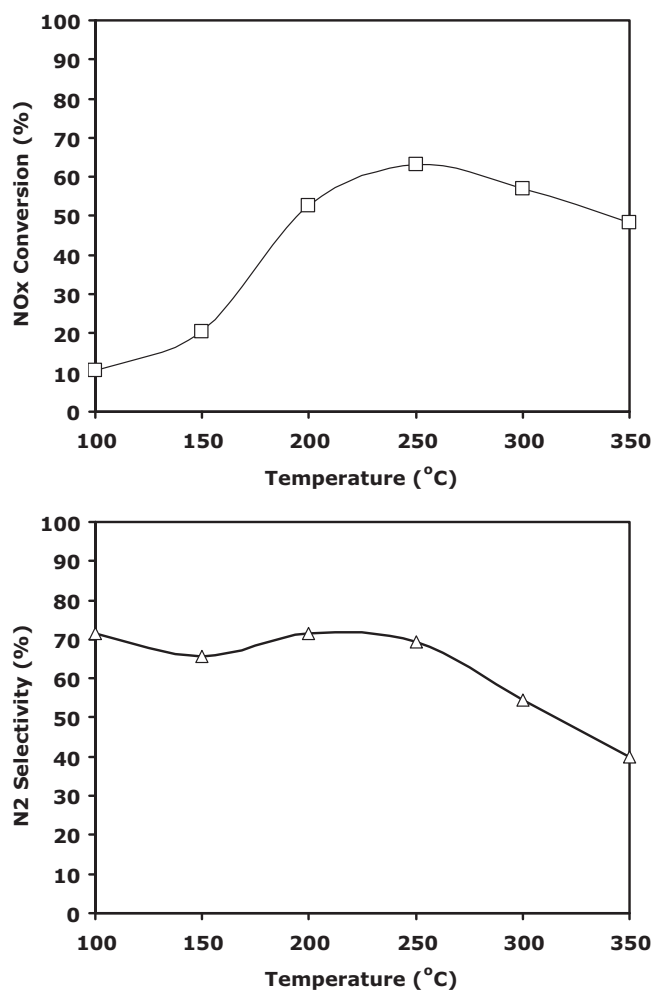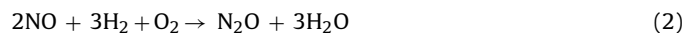
Fig. 7. NO_x conversion and N_2 selectivity over Zn-ZSM-5 as a function of temperature. Reaction condition: 200 ppm NO, 3000 ppm H_2, 1.5% O_2, balance helium, 0.2 g catalyst, flow rate 100 mL/min.

decreased when temperature increased to 350 °C (Fig. 7). It is noted that the N_2 selectivity dropped when NO concentration in the feed was increased from 50 to 200 ppm. As shown below, during the reaction, the main reactions taking place in the $NO/H_2/O_2$ system are:

$$2NO + 4H_2 + O_2 \rightarrow N_2 + 4H_2O \tag{1}$$

$$2NO + 3H_2 + O_2 \rightarrow N_2O + 3H_2O \tag{2}$$

$$O_2 + 2H_2 \rightarrow 2H_2O \tag{3}$$

when more NO was added, reaction (2) was favored. More N_2O (~19 ppm) was generated leading in a drop in N_2 selectivity.

3.3. Comparison of NO_x reduction on Zn-ZSM-5, Pd/Zn-ZSM-5 and $Pd/Ru/W/(ZrO_2-SiO_2)SO4$ catalysts

To compare the H_2-SCR activities over Zn-ZSM-5 with other conventional catalysts, two noble metal catalysts Pd/Zn-ZSM-5 and $Pd/Ru/W/(ZrO_2-SiO_2)SO_4$ (an industrial catalyst [51]) were also synthesized and evaluated as nanoparticles catalyst. The XRD patterns of Pd/Zn-ZSM-5 and $Pd/Ru/W/(ZrO_2-SiO_2)SO_4$ are shown in Fig. S5. The obtained Pd/Zn-ZSM-5 samples exhibited the characteristic peaks associated with MFI structure, indicating the zeolite structure was retained after the Pd doping process. Crystalline PdO phases were not detected from the XRD pattern, which indicated that Pd was highly dispersed on Zn-ZSM-5
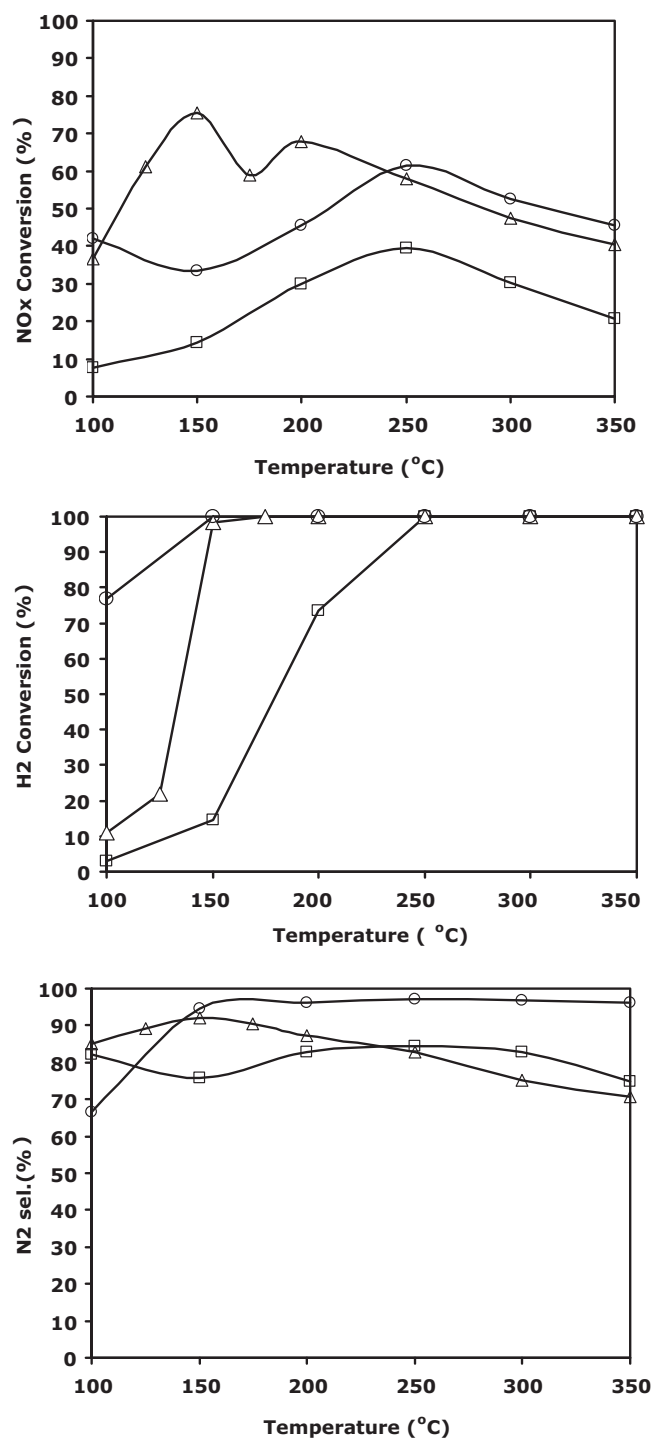

Fig. 8. NO_x conversion, hydrogen conversion and N_2 selectivity over 0.25 g $Pd/Ru/W/(ZrO_2-SiO_2)SO_4$ (△), 0.2 g Pd/Zn-ZSM-5(○), and 0.2 g Zn-ZSM-5(□). Reaction condition: 50 ppm NO, 2000 ppm H_2, 1.5% O_2, balance helium, flow rate 200 mL/min.

support. For $Pd/Ru/W/(ZrO_2-SiO_2)SO_4$ sample, intense diffraction peaks assigned to tetragonal and monoclinic zirconia phases were observed. The low peak intensities of Pd and Ru were due to the high dispersion of these metals and their low doping amounts in the catalysts (0.8% Pd and 0.11% Ru). The N_2 adsorption isotherm of Pd/Zn-ZSM-5 is typical type I isotherm and its BET surface area is 390 m^2/g, which is slightly lower than that of Zn-ZSM-5 (Fig. S6). While the BET surface area of $Pd/Ru/W/(ZrO_2-SiO_2)SO_4$ is 50 m^2/g, which is typical for $(ZrO_2-SiO_2)SO_4$ based catalysts (Fig. S5).

NO$_x$ reduction over Zn-ZSM-5, Pd/Zn-ZSM-5 and Pd/Ru/W/(ZrO$_2$–SiO$_2$)SO$_4$ catalysts is compared in Fig. 8. In the entire temperature range, Pd/Zn-ZSM-5 and Pd/Ru/W/(ZrO$_2$–SiO$_2$)SO$_4$ showed higher NO$_x$ conversions than Zn-ZSM-5. The higher activities were mainly due to the noble metals used in these two catalysts, which improved the utilization of H$_2$ more than Zn did. Comparison of hydrogen conversion as a function of temperature over Zn-ZSM-5, Pd/Zn-ZSM-5 and Pd/Ru/W/(ZrO$_2$–SiO$_2$)SO$_4$ catalysts also confirmed this observation. As shown in Fig. 8, 100% H$_2$ conversion over Pd/Zn-ZSM-5 and Pd/Ru/W/(ZrO$_2$–SiO$_2$)SO$_4$ occurred at 150 °C, while that over Zn-ZSM-5 occurred at 250 °C. Clearly, noble metals containing catalysts are more active than Zn-ZSM-5 at lower temperatures. This also explained the higher NO$_x$ conversions over Pd/Zn-ZSM-5 and Pd/Ru/W/(ZrO$_2$–SiO$_2$)SO$_4$ than that over Zn-ZSM-5 at lower temperatures (≤150 °C). The high activities observed on Pd/Zn-ZSM-5 and Pd/Ru/W/(ZrO$_2$–SiO$_2$)SO$_4$ catalysts at low temperatures were also consistent with the previous work reported by Ueda et al. and Macleod and Lambert [26,31]. It is worth noting that Zn-ZSM-5 had only one NO$_x$ conversion peak. The NO$_x$ conversion increased with temperature and reached the maximum conversion of 39.5% at 250 °C. Under the same conditions, Pd/Zn-ZSM-5 catalyst exhibited a higher NO$_x$ conversion of 61.4% at 250 °C. The high conversion over Pd/Zn-ZSM-5 at 250 °C was probably due to the combined contributions from Pd and Zn at this temperature. For Pd/Ru/W/(ZrO$_2$–SiO$_2$)SO$_4$ catalyst, two NO$_x$ conversion peaks at 150 and 200 °C were also observed. The maximum NO$_x$ conversion over Pd/Ru/W/(ZrO$_2$–SiO$_2$)SO$_4$ was 75.5% at 150 °C. N$_2$ selectivities over the three catalysts were also compared in Fig. 8. N$_2$ was the main product for NO$_x$ reduction over these three catalysts. N$_2$ selectivities ranging from 70% to 90% were obtained on Zn-ZSM-5 and Pd/Ru/W/(ZrO$_2$–SiO$_2$)SO$_4$. The highest N$_2$ selectivity of >95% was obtained on Pd/Zn-ZSM-5 when the temperature was raised to higher than 150 °C.

3.4. Effect of CO concentration on NO$_x$ reduction

To study the effect of CO concentration on NO$_x$ reduction over Zn-ZSM-5, Pd/Zn-ZSM-5 and Pd/Ru/W/(ZrO$_2$–SiO$_2$)SO$_4$ catalysts, CO with concentrations varying from 500 to 2000 ppm was added to the feed gas. The SCR reaction temperature was set to 250 °C, where all the three catalysts have shown a NO conversion peak. As shown in Fig. 9, NO$_x$ conversion decreased slightly with increased CO concentration over Zn-ZSM-5: NO$_x$ conversion over Zn-ZSM-5 decreased from 39.5% at 0 ppm CO to 31.1% at 2000 ppm CO. When Zn-ZSM-5 is exposed to CO for longer amount of time, i.e., 5 h, no obvious reduction in activity was observed after 2 h of reaction. For Pd/Zn-ZSM-5, the same trend that NO$_x$ conversion decreasing with CO concentration was observed. NO$_x$ conversion over Pd/Zn-ZSM-5 was more influenced by the presence of CO. In the presence of 2000 ppm CO, there was a 13.7% decrease in NO$_x$ conversion over Pd/Zn-ZSM-5. For Pd/Ru/W/(ZrO$_2$–SiO$_2$)SO$_4$ catalyst, a decrease from 49.5% at 0 ppm CO to 41.6% at 2000 ppm CO was observed. There were studies which showed that the presence of CO had a noticeable inhibiting effect on NO$_x$ reduction and the inhibition effect increased with CO concentration [41–45]: CO poisoning effect was attributed to the competitive adsorption between CO and NO on the same active sites and CO strong competition for hydrogen adsorption sites on metal catalyst which caused the lower surface coverage of hydrogen.

The effect of CO on N$_2$ selectivity over Zn-ZSM-5, Pd/Zn-ZSM-5 and Pd/Ru/W/(ZrO$_2$–SiO$_2$)SO$_4$ catalysts was also studied. As shown in Fig. 9, upon adding low concentration CO to the feed gas, such as 500 ppm, N$_2$ selectivity over Zn-ZSM-5 increased to nearly 90%. A further increase in CO concentration caused a decrease in the selectivity, and the N$_2$ selectivity in the presence of 2000 ppm CO decreased to the same level as that in the
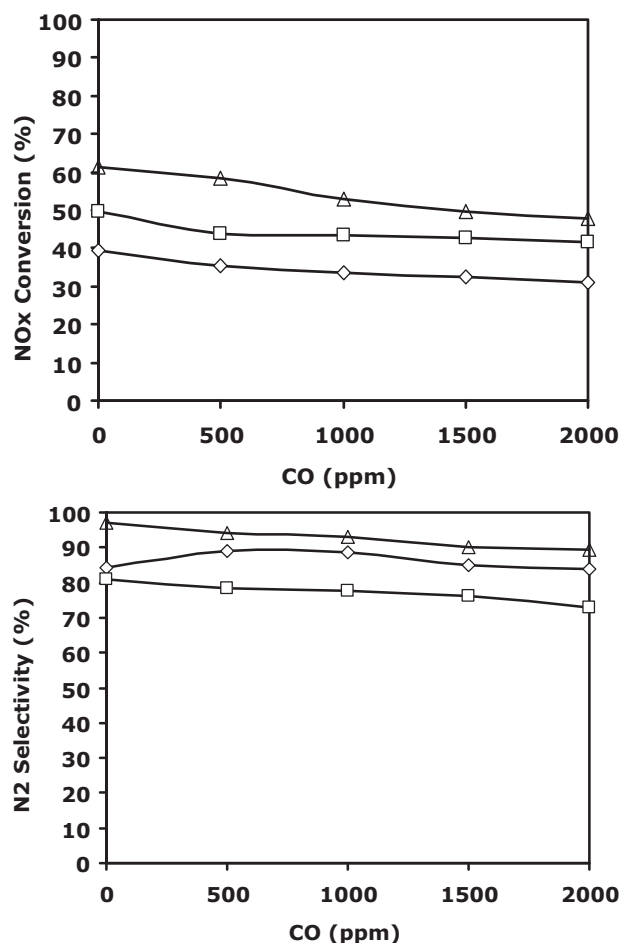

Fig. 9. Effects of CO concentration on NO conversion and N$_2$ selectivity at 250 °C over Pd/Ru/W/(ZrO$_2$–SiO$_2$)SO$_4$ (□), Pd/Zn-ZSM-5 (△) and Zn-ZSM-5 (◇). Reaction condition: 50 ppm NO, 2000 ppm H$_2$, 1.5% O$_2$, 0–2000 ppm CO, balance helium, 0.2 g catalyst, flow rate 200 mL/min.

absence of CO. As for Pd/Zn-ZSM-5 and Pd/Ru/W/(ZrO$_2$–SiO$_2$)SO$_4$, continuous decrease in N$_2$ selectivity with CO concentration was observed.

3.5. Effect of water vapor on NO$_x$ reduction

Studying the effect of water vapor is important since water generally caused catalyst deactivation in commercial applications. The effects of H$_2$O on activities of Zn-ZSM-5, Pd/Zn-ZSM-5 and Pd/Ru/W/(ZrO$_2$–SiO$_2$)SO$_4$ were evaluated at 250 °C in the presence of 1000 ppm CO (i.e., H$_2$/CO = 2). As shown in Fig. 10, in the presence of 17.5% H$_2$O and 1000 ppm CO, NO$_x$ conversion over Zn-ZSM-5 decreased from 33.7% to 29.3% after 1 h and stabilized at 26% after 5 h on stream. For Pd/Zn-ZSM-5 and Pd/Ru/W/(ZrO$_2$–SiO$_2$)SO$_4$, NO$_x$ conversion also decreased in the presence of water vapor. It decreased from 52.8% to 39.7% over Pd/Zn-ZSM-5 and from 43.6% to 37.4% over Pd/Ru/W/(ZrO$_2$–SiO$_2$)SO$_4$ after 5 h on stream. N$_2$ selectivity was not affected much by water vapor, as shown in Fig. 10.

3.6. Effect of SO$_2$ on NO$_x$ reduction

Because resistance to sulfur poisoning is an important factor in the applications for SCR catalysts, we studied the effect of SO$_2$ on the catalytic performance over the three catalysts. The effect of SO$_2$ on SCR activity in the presence of 1000 ppm CO and 17.5% H$_2$O is illustrated in Fig. 11. At 250 °C, when 7.5 ppm SO$_2$ was added to the feed gas, NO conversion over Zn-ZSM-5 decreased rapidly from 27.6% to
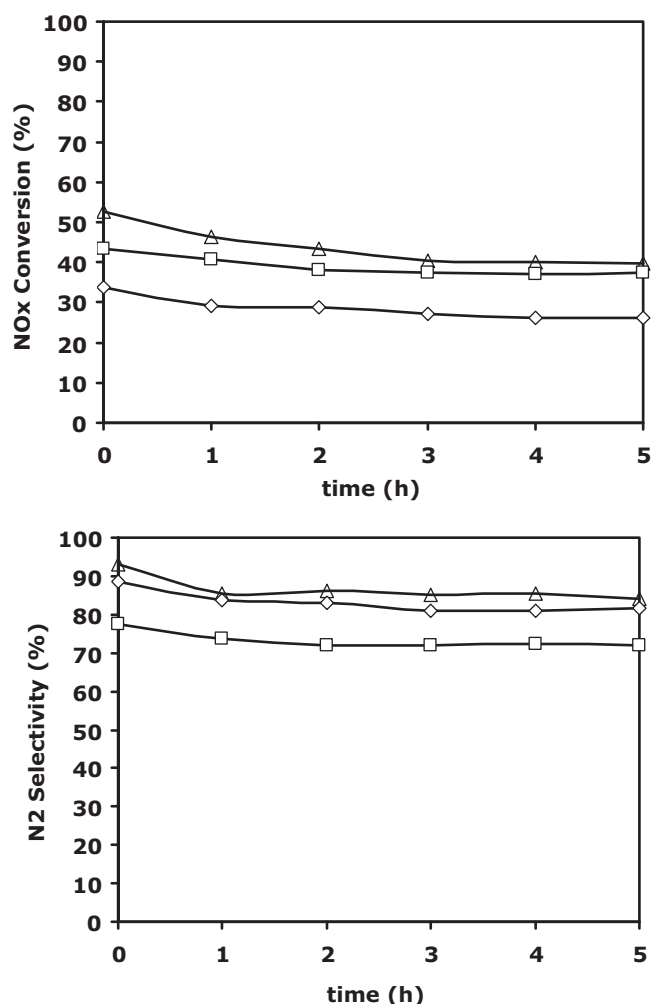
Fig. 10. Effects of water vapor on NO conversion and N_2 selectivity at 250 °C over Pd/Ru/W/(ZrO$_2$–SiO$_2$)SO$_4$ (□), Pd/Zn-ZSM-5 (△) and Zn-ZSM-5 (◇). Reaction condition: 50 ppm NO, 2000 ppm H$_2$, 1.5% O$_2$, 1000 ppm CO, 17.5% H$_2$O, balance helium, 0.2 g catalyst, flow rate 200 mL/min.
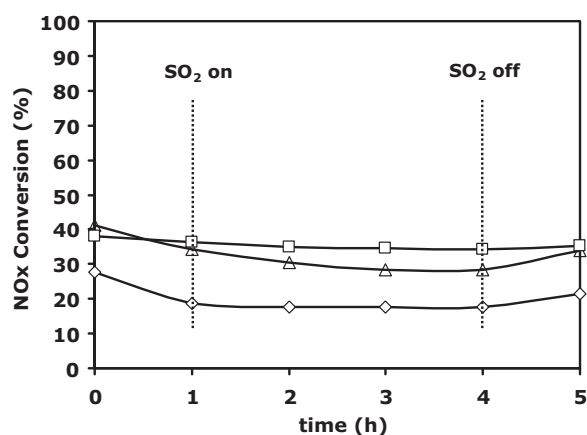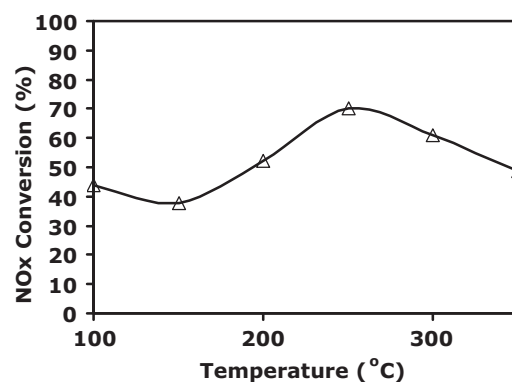

Fig. 12. NO$_x$ conversion over Pd/Zn-ZSM-5-plasma. Reaction condition: 50 ppm NO, 2000 ppm H$_2$, 1.5% O$_2$, balance helium, flow rate 200 mL/min, 0.2 g catalyst.

17.3% in the first four hours while longer SO$_2$ time exposure (three additional hours) only decreased NO conversion to 16.1% suggesting that most of the poisoning occurred during the first four hours. Nearly 80% activity was restored after SO$_2$ feed was removed. A further regeneration of the catalyst in air at 500 °C for 5 h restored the activity to 90%. For Pd/Zn-ZSM-5, the same trend that NO$_x$ conversion decreased with SO$_2$ addition was also observed (a 13% decrease) and removal of SO$_2$ feed restored the activity to ~83%. However, for Pd/Ru/W/(ZrO$_2$–SiO$_2$)SO$_4$, only a slight decrease in its SCR activity was observed. Compared with the SO$_2$ influence on Zn-ZSM-5 and Pd/Zn-ZSM-5, Pd/Ru/W/(ZrO$_2$–SiO$_2$)SO$_4$ was less poisoned by SO$_2$. This was likely due to the superacidic nature of (ZrO$_2$)SO$_4$ support [60].

3.7. NO$_x$ reduction on Pd/Zn-ZSM-5-plasma treated by Ar plasma

We also synthesized Pd/Zn-ZSM-5-plasma by using the glow discharge plasma reduction route. Compared to Pd/Zn-ZSM-5 synthesized by conventional method, Pd/Zn-ZSM-5-plasma treated with Ar plasma showed enhanced NO$_x$ reduction activities (Fig. 12). NO$_x$ conversion reached 70.2% at 250 °C. It is known that plasma treatment techniques are effective in preparing highly dispersed, supported metal catalysts as well as improving the metal-support interactions, and its application in catalyst preparation has been previously reviewed [61]. The high dispersion of metals reduced
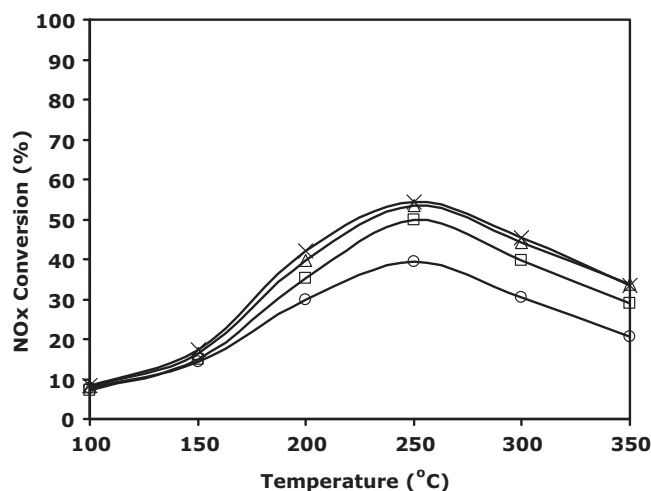

Fig. 11. Effect of SO$_2$ on NO conversion at 250 °C over Pd/Ru/W/(ZrO$_2$–SiO$_2$)SO$_4$ (□), Pd/Zn-ZSM-5 (△) and Zn-ZSM-5 (◇). Reaction condition: 50 ppm NO, 2000 ppm H$_2$, 1.5% O$_2$, 1000 ppm CO, 17.5% H$_2$O, 7.5 ppm SO$_2$, balance helium, 0.2 g catalyst, flow rate 200 mL/min.

Fig. 13. NO$_x$ conversion over Zn-ZSM-5 (ion exchanged once: ○, exchange 2×: □ exchange 3×: △, exchange 4×: ×). Reaction condition: 50 ppm NO, 2000 ppm H$_2$, 1.5% O$_2$, balance helium, flow rate 200 mL/min.
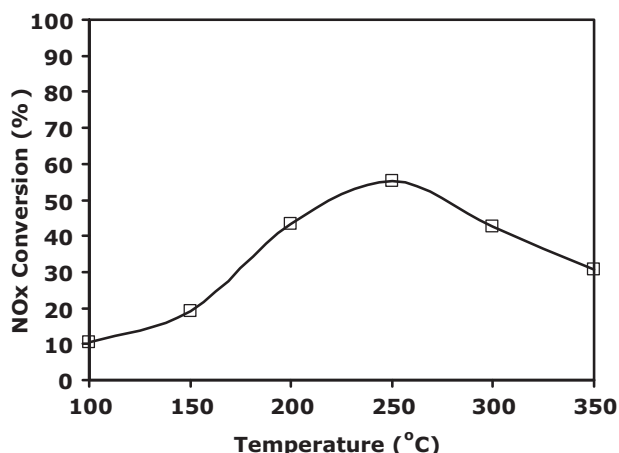
Fig. 14. NO$_x$ conversion over Zn-ZSM-5 (after ion-exchange four times, the sample was further doped with 2 wt% ZnO via incipient wetness impregnation). Reaction condition: 50 ppm NO, 2000 ppm H$_2$, 1.5% O$_2$, balance helium, flow rate 200 mL/min.

by plasma would enhance the utilization efficiency of metals. Liu's group has reported that metal-doped catalysts prepared by glow discharge plasma reduction showed higher activities [62–64]. Researchers also found that plasma treatment can significantly change the structure of the supported metal and the metal-support interactions [65,66].

3.8. Optimization of Zn-ZSM-5

Compared to conventional noble metal supported catalysts, the activity of Zn-ZSM-5 was relatively low. We optimized the ion-exchange procedure for Zn-ZSM-5 and studied the NO$_x$ reduction over Zn-ZSM-5 samples with various % ion exchanged. As shown in Fig. 13, NO$_x$ conversions increased from 39.5% over Zn-ZSM-5 (ion exchanged once) to 49.7% over Zn-ZSM-5-2 (ion exchanged twice), and to 53.5% over Zn-ZSM-5-3 (ion exchanged three times), then leveled off at 54.3% for Zn-ZSM-5-4 (exchanged four times). EDX results showed that Zn contents in these Zn-ZSM-5 samples were 1.17% for Zn-ZSM-5-1, 1.64% for Zn-ZSM-5-2, 1.9% for Zn-ZSM-5-3, and 1.95% for Zn-ZSM-5-4. More Zn cations are favorable for higher activities of Zn-ZSM-5. N$_2$ selectivity over Zn-ZSM-5-4 showed that there was no obvious effect of Zn content on N$_2$ selectivity (Fig. S7). To further study the Zn effect on NO conversion, a Zn-ZSM-5-5 was synthesized by further incipient wetness impregnation of Zn-ZSM-5-4 with Zn(NO$_3$)$_2$ to dope ~2 wt% ZnO. As shown Fig. 14,
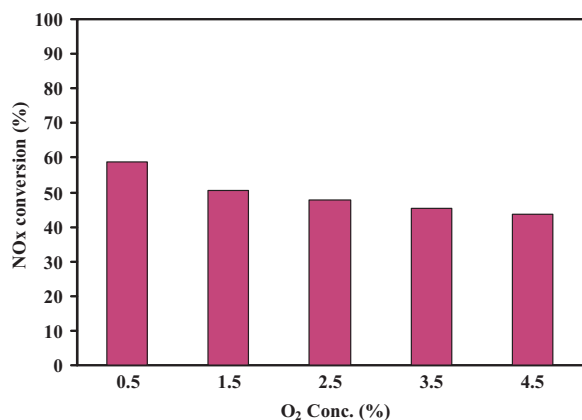

Fig. 15. NO$_x$ conversion over Zn-ZSM-5. Reaction condition: 50 ppm NO, 2000 ppm H$_2$, various O$_2$ concentrations, balance helium, flow rate 200 mL/min, 0.2 g catalyst, 250 °C.

NO$_x$ conversion over Zn-ZSM-5-5 was 55.1%. There was no clear increase in NO$_x$ conversion when compared with Zn-ZSM-5-4. The results indicated that ZnO did not contribute to NO reduction.

3.9. Oxygen effect on NO$_x$ conversion over Zn-ZSM-5

The effects of O$_2$ concentration on NO$_x$ reduction over Zn-ZSM-5-2 were studied by varying oxygen concentrations from 0.5% to 4.5% in the feed gas. The SCR reaction temperature was set to 250 °C, where the catalyst showed a NO conversion peak. As shown in Fig. 15, NO$_x$ conversion decreased with increased oxygen concentration over Zn-ZSM-5. NO$_x$ conversion over Zn-ZSM-5 decreased from 58.6% at 0.5% oxygen to 43.8% at 4.5% oxygen. These results suggest that oxygen competed with NO to react with hydrogen.

4. Conclusions

This work has demonstrated that Zn-ZSM-5 catalyst, as a non-noble metal containing catalyst, was active for the SCR reaction of NO with hydrogen. The activity of Zn-ZSM-5 catalyst was attributed to the presence of Zn cations in the framework. TPD results showed that the binding of the chemisorbed hydrogen on Zn-ZSM-5 increased with temperature and both Zn cations and the zeolite framework affected the hydrogen chemisorption. As compared with two conventional noble metal supported catalysts, Pd/Zn-ZSM-5 and Pd/Ru/W/(ZrO$_2$–SiO$_2$)SO$_4$, Zn-ZSM-5 showed one NO$_x$ conversion peak at 250 °C, where ~100% H$_2$ conversion over Zn-ZSM-5 was observed. CO concentration, water vapor and SO$_2$ were all found to lower the SCR activities over Zn-ZSM-5, Pd/Zn-ZSM-5 and Pd/Ru/W/(ZrO$_2$–SiO$_2$)SO$_4$. In addition, we also synthesized Pd/Zn-ZSM-5-plasma by using the glow-discharge plasma-reduction route. Compared to Pd/Zn-ZSM-5 synthesized by conventional method, H$_2$-SCR activities of Pd/Zn-ZSM-5-plasma were further enhanced by the plasma reduction route. The ion-exchange procedure for Zn-ZSM-5 was also optimized for enhanced NO$_x$ conversions. Effects of O$_2$ concentration on Zn-ZSM-5 activity were also shown. Our findings of Zn-ZSM-5 as an active catalyst for H$_2$-SCR reaction could offer new thinking for designing novel, low-cost, non-noble-metal catalysts for H$_2$-SCR.

Appendix A. Supplementary data

Supplementary data associated with this article can be found, in the online version, at http://dx.doi.org/10.1016/j.apcatb.2014.01.036.

References

[1] Y. Cai, U.S. Ozkan, Int. J. Energy Environ. Econ. 1 (1991) 229–236.
[2] Y. Cai, U.S. Ozkan, Appl. Catal. 78 (1991) 241–255.
[3] U.S. Ozkan, Y. Cai, M.W. Kumthekar, Appl. Catal., A 96 (1993) 365–381.
[4] M.W. Kumthekar, U.S. Ozkan, Appl. Catal., A 151 (1997) 289–303.
[5] E.Y. Choi, I.-S. Nam, Y.G. Kim, J. Catal. 161 (1996) 597–604.
[6] H.J. Chae, I.-S. Nam, S.-W. Ham, S.B. Hong, Appl. Catal., B 53 (2004) 117–126.
[7] J.W. Choung, I.-S. Nam, Appl. Catal., B 64 (2006) 42–50.
[8] Y.J. Kim, H.J. Kwon, I. Heo, I.-S. Nam, B.K. Cho, J.W. Choung, M.-S. Cha, G.K. Yeo, Appl. Catal., B 126 (2012) 9–21.
[9] J. Wang, T. Yu, X. Wang, G. Qi, J. Xue, M. Shen, W. Li, Appl. Catal., B 127 (2012) 137–147.
[10] L. Wang, W. Li, G. Qi, D. Weng, J. Catal. 289 (2012) 21–29.
[11] J. Xue, X. Wang, G. Qi, Jun Wang, M. Shen, W. Li, J. Catal. 297 (2013) 56–64.
[12] A. Fritz, V. Pitchon, Appl. Catal., B 13 (1997) 1–25.
[13] H. Bosch, F. Janssen, Catal. Today 2 (1988) 369–532.
[14] G. Busca, L. Lietti, G. Ramis, F. Berti, Appl. Catal., B 18 (1998) 1–36.

[15] L.J. Lobree, I-C. Hwang, J.A. Reimer, A.T. Bell, J. Catal. 186 (1999) 242–253.
[16] R.Q. Long, R.T. Yang, J. Am. Chem. Soc. 121 (1999) 5595–5596.
[17] R.Q. Long, R.T. Yang, J. Catal. 188 (1999) 332–339.
[18] R.Q. Long, R.T. Yang, J. Catal. 198 (2001) 20–28.
[19] G. Qi, R.T. Yang, J. Catal. 217 (2003) 434–441.
[20] G. Qi, J.E. Gatt, R.T. Yang, J. Catal. 226 (2004) 120–128.
[21] R. Qu, X. Gao, K. Cen, J.H. Li, Appl. Catal., B 142–143 (2013) 290–297.
[22] Y. Peng, C. Liu, X. Zhang, J.H. Li, Appl. Catal., B 140–141 (2013) 276–282.
[23] S. Brandenberger, O. Krocher, A. Tissler, R. Althoff, Catal. Rev. 50 (2008) 492–531.
[24] P. Granger, V.I. Parvulescu, Chem. Rev. 111 (2011) 3155–3207.
[25] W.C. Hecker, A.T. Bell, J. Catal. 92 (1985) 247–259.
[26] A. Ueda, N. Takayuki, A. Masashi, T. Kobayashi, Catal. Today 45 (1998) 135–138.
[27] K. Yokota, M. Fukui, T. Tanaka, Appl. Surf. Sci. 121–122 (1997) 273–277.
[28] R. Burch, M.D. Coleman, Appl. Catal., B 23 (1999) 115–121.
[29] C.N. Costa, V.N. Stathopoulos, V.C. Belessi, A.M. Efstathiou, J. Catal. 197 (2001) 350–364.
[30] C.N. Costa, P.G. Savva, C. Andronikou, P.S. Lambrou, K. Polychronopoulou, V.C. Belessi, V.N. Stathopoulos, P.J. Pomonis, A.M. Efstathiou, J. Catal. 209 (2002) 456–471.
[31] N. Macleod, R.M. Lambert, Catal. Commun. 3 (2002) 61–65.
[32] R. Burch, M.D. Coleman, J. Catal. 208 (2002) 435–447.
[33] M. Machida, S. Ikeda, D. Kurogi, T. Kijima, Appl. Catal., B 35 (2001) 107–116.
[34] J. Shibata, M. Hashimoto, K. Shimizu, H. Yoshida, T. Hattori, A. Satsuma, J. Phys. Chem. B 108 (2004) 18327–18335.
[35] M. Machida, T. Watanabe, Appl. Catal., B 52 (2004) 281–286.
[36] G. Qi, R.T. Yang, L.T. Thompson, Appl. Catal., A 259 (2004) 261–267.
[37] G. Qi, R.T. Yang, F.C. Rinaldi, J. Catal. 237 (2006) 381–392.
[38] C.N. Costa, A.M. Efstathiou, Appl. Catal., B 72 (2007) 240–252.
[39] P. Wu, L. Li, Q. Yu, G. Wu, N. Guan, Catal. Today 158 (2010) 228–234.
[40] H. Hamada, M. Haneda, Appl. Catal., A 421–422 (2012) 1–13.
[41] K. Yokota, M. Fukui, T. Tanaka, Appl. Surf. Sci. 121–122 (1997) 273–277.
[42] G.C. Mondragon Rodrıguez, B. Saruhan, Appl. Catal., B 93 (2010) 304–313.
[43] C.N. Costa, P.G. Savva, J.L.G. Fierro, A.M. Efstathiou, Appl. Catal., B 75 (2007) 147–156.
[44] P.G. Savva, C.N. Costa, Catal. Rev. Sci. Eng. 53 (2011) 91–151.
[45] Z. Liu, J. Li, S.I. Woo, Energy Environ. Sci. 5 (2012) 8799–8814.
[46] J.A. Biscardi, E. Iglesia, J. Catal. 182 (1999) 117–128.
[47] J.A. Biscardi, G.D. Meitzner, E. Iglesia, J. Catal. 179 (1998) 192–202.
[48] V.B. Kazansky, J. Catal. 216 (2003) 192–202.
[49] V.B. Kazansky, A.I. Serykh, B.G. Anderson, R.A. van Santen, Catal. Lett. 88 (2003) 211–217.
[50] V.B. Kazansky, A.I. Serykh, Phys. Chem. Chem. Phys. 6 (2004) 3760–3764.
[51] A. Sobolevskiy, J.A. Rossin, M.J. Knapke, US Patent 7,976,805 B2, 2011.
[52] A.J. Lachawiec, R.T. Yang, J. Phys. Chem. C 113 (2009) 13933–13939.
[53] L.F. Wang, N.R. Stuckert, R.T. Yang, AIChE J. 57 (2011) 2902–2908.
[54] L.F. Wang, N.R. Stuckert, H. Chen, R.T. Yang, J. Phys. Chem. C 115 (2011) 4793–4799.
[55] G.W. Busser, O. Hinrichsen, M. Muhler, Catal. Lett. 79 (2002) 49–54.
[56] F.G. Wei, T. Hara, K. Tsuzaki, Metall. Mater. Trans. B 35 (2004) 587.
[57] V.R. Choudhary, K. Mantri, Microporous Mesoporous Mater. 40 (2000) 127–133.
[58] R.I. Masel, Principles of Adsorption and Reaction on Solid Surfaces, Wiley, 1996.
[59] L.A.M.M. Barbosa, R.A. van Santen, J. Phys. Chem. C 111 (2007) 8337–8348.
[60] Y. Wang, J. Ma, D. Liang, M. Zhou, F. Li, R. Li, J. Mater. Sci. 44 (2009) 6736–6740.
[61] C.J. Liu, G.P. Vissokov, B.W.L. Jang, Catal. Today 72 (2002) 173–184.
[62] Z. Wang, C.J. Liu, G.L. Zhang, Catal. Commun. 10 (2009) 959–962.
[63] Z.-J. Wang, Y.-B. Xie, C.-J. Liu, J. Phys. Chem. C 112 (2008) 19818–19824.
[64] L. Xi, C.-J. Liu, Y.P. Zhang, P.-Y. Kuai, Green Chem. 10 (2008) 1318–1322.
[65] C. Ratanatawanate, M. Monyka, B.W.-L. Jang, Ind. Eng. Chem. Res. 44 (2005) 9868–9874.
[66] J.-J. Zou, C.-J. Liu, Y.-P. Zhang, Langmuir 22 (2006) 2334–2339.